Surface freezing in *n*-alkane solutions: The relation to bulk phases

E. Sloutskin,[1] E. B. Sirota,[2] H. Kraack,[1] B. M. Ocko,[3] and M. Deutsch[1,*]

[1]*Physics Department, Bar Ilan University, Ramat Gan 52900, Israel*
[2]*ExxonMobil Research and Engineering Co., Route 22 E., Annandale, New Jersey 08801*
[3]*Physics Department, Brookhaven National Laboratory, Upton, New York 11973*
(Received 28 February 2001; published 29 August 2001)

Surface freezing (SF) was investigated in tricosane-dodecane alkane solutions as a function of temperature (T) and molar concentration of tricosane (ϕ), using surface tension and synchrotron x-ray surface diffraction techniques. A crystalline SF monolayer, having a rotator R_{II} structure, was found to exist for $35\,°\mathrm{C} \leq T \leq 50\,°\mathrm{C}$ and $0.3 \leq \phi \leq 1$. The extended temperature range allowed to determine the linear-expansion coefficient of the SF monolayer, $(dd/dT)/d = 6.5 \times 10^{-4}\,°\mathrm{C}^{-1}$. A simple thermodynamical model based on the theory of ideal solutions is shown to account well for the ϕ dependence of the SF temperature $T_s(\phi)$. The study shows that the temperature range of existence of the surface frozen layer at each ϕ, the ϕ range over which SF is observed, and the bulk solidification behavior, are intimately related. All are determined by the rotator-liquid dissolution line $T_{dR}(\phi)$.

I. INTRODUCTION

Normal alkanes, having the molecular structure $\mathrm{H(CH_2)}_n\mathrm{H}$ (denoted C_n in the following), are among the most important building blocks of organic matter [1]. They are linear molecules having a planar zigzag conformation with a carbon atom at each vertex as their ground state. Their properties in the liquid and solid phase have been extensively investigated. Their bulk phase diagram reveals a series of plastic-crystalline phases intruding between the liquid and crystalline phase. The structure in these phases is lamellar, with a long-range positional order of the molecular center-of-mass, but only short-range order in the angle of rotation of the molecular plane around the long axis of the molecules. Hence their name: rotator phases [2–9]. The orthorhombic crystalline phases of alkanes have a herringbone order in the azimuthal angle of rotation [10–12]. Five rotator phases have been identified, differing in the in-plane packing symmetry and the tilt angle and direction [2,7]. The highest-symmetry rotator phase is the R_{II} phase, which is hexagonally packed, with the molecules aligned normal to the lamellar plane.

Alkanes show another peculiar property. In accordance with general thermodynamical principles, solids of all materials undergo surface melting; their free surfaces melt, in general, at a temperature lower than, or equal to that of the bulk. Surprisingly, alkanes and several of their derivatives were found a few years ago to undergo an opposite effect, surface *freezing* (SF) [13–25]. Here the surface layer of the melt solidifies at a temperature T_s *higher* than that of the bulk T_f. In alkanes, the surface-frozen layer is one molecule thick, and, for chain lengths $16 \leq n \leq 30$, the SF monolayer has a structure identical with that of a single R_{II} lamella [13]. The surface-freezing range, $\Delta T_{SF} = T_s - T_f$, is, however, rather narrow, usually $\leq 3\,°\mathrm{C}$. Thus, the temperature dependence of the SF layer properties can be studied over only a very limited range. Moreover, this short temperature range

does not allow reaching any phase transitions in the surface-frozen layer of any pure alkane. Thus, relations between the surface and bulk phase diagrams cannot be studied, in spite of the strong evidence for an intimate connection between SF and bulk nucleation, provided by our recent bulk homogeneous and heterogeneous nucleation experiments [26–28] and other studies [29–32].

An efficient way of studying these issues over an extended temperature range is provided by solutions of long-chains in short-chain alkanes. By varying the molar concentration ϕ of the long-chain alkane, it is possible to tune the chemical-potential balance and reach regions in the phase space not accessible with the pure material. This is true for both the bulk and the surface. Indeed, a temperature-or-concentration induced phase transition between a rotator and a crystal phase was found in the SF monolayer of binary alkane mixtures [15]. A recent study of the bulk phase behavior of C_{23}/C_{12} mixtures [31] shows a crossover, with decreasing ϕ, from a rotator-to-liquid dissolution to a crystal-to-liquid dissolution, at temperatures T_{dR} and T_{dX}, respectively. An accompanying transition from a nonsupercooling to a supercooling bulk behavior was also found. The lower supercooling temperature was shown to follow an extrapolation of the rotator-liquid dissolution line, T_{dR}, below the crossover concentration of $\phi \approx 0.6$.

To explore the relation between the bulk and surface phase diagrams, we have undertaken a study of the concentration and the temperature dependence of surface freezing in C_{23}/C_{12} solutions, using both surface tension and surface-specific synchrotron x-ray techniques. The x-ray measurements show that no structural phase transitions occur in the surface-frozen layer over the full temperature ($35\,°\mathrm{C} \leq T \leq 50\,°\mathrm{C}$) and concentration ($0.3 \leq \phi \leq 1$) ranges over which equilibrium SF exists in these mixtures. However, this paper clearly demonstrates that the SF existence range at each ϕ is dominated by the nonlinear variation of the bulk freezing temperature T_{dR}, with $\ln(\phi)$. We also show that the vanishing of the SF effect is caused by the pre-emption of the $T_s(\phi)$ line by the $T_{dR}(\phi)$ line. Although these two lines start

---

*Corresponding author. Email address: deutsch@mail.biu.ac.il

out being parallel at $\phi \approx 1$, the R_I and R_V rotator bulk phases, occurring at temperatures below the uppermost solid R_{II} rotator phase in C_{23} [7], induce an upward curvature to $T_{dR}[\ln(\phi)]$. By contrast, the absence of such phases at the surface-frozen layer renders $T_s[\ln(\phi)]$ linear. These different behaviors lead to an intersection of the two lines at low ϕ, and the vanishing of the SF effect. A simple thermodynamic model, based on the theory of ideal solutions and closely related to a similar theory, which explains the bulk behavior [31], is shown to account well for the T and ϕ dependence of $T_s(\phi)$. The x-ray grazing incidence diffraction results allow an accurate determination of the expansion coefficient of the surface-frozen layer.

In Sec. II we briefly present the experimental techniques and procedures, with Sec. III presenting and discussing the results obtained.

II. EXPERIMENT

The surface structure was studied by x-ray reflectivity (XR) and grazing incidence diffraction (GID). The surface thermodynamics were studied using surface tension (ST) measurements. The experimental methods have already been described in detail [13,14,16,33]. Only a brief summary will be given here, concentrating mostly on features peculiar to this study.

A. Samples

Materials purchased from Fluka, Aldrich, and Sigma, were designated as $\geq 99\%$ pure, and used as obtained. The mixtures were prepared by weighing the required amounts for a total volume of 0.3 cm³ (ST) or 0.7 cm³ (x rays), heating them well above the melting temperature of C_{23}, and stirring vigorously on a hotplate with a magnetic stirrer for >10 min in a closed container. Samples were always loaded into the ST or x-ray cells without allowing them to freeze prior to the measurement run, to minimize the danger of demixing and phase separation.

B. X-ray measurements

The x-ray measurements were carried out at the Harvard/ BNL liquid surface diffractometer at the beamline X22B, National Synchrotron Light Source, Brookhaven National Laboratory, using x rays of wavelength 1.57 Å. The ≤ 1 g liquid sample was poured onto a 5 cm diam thin copper wafer, yielding a 0.5 mm deep puddle covering the wafer. The wafer sat inside a two-stage oven. The temperature of the inner cell of the oven was controlled electronically to $\leq 0.005\,°C$. The outer, passive, enclosure had Kapton windows. The inner, temperature-controlled, thin walled cell was machined from solid beryllium, with top and bottom copper flanges carrying the thin-film heaters and thermistors used for controlling the temperature. Since the free volume of the cell was very small and the cell was sealed throughout the measurements, water adsorption by the slightly hygroscopic C_{12} was negligible. The inner cell could be cooled below ambient by a heat exchanger attached to its bottom, through

which water with a fixed temperature ($\pm 0.1\,°C$) could be circulated by a Neslab refrigerated bath.

The surface-normal density profile of the vapor-liquid interface was explored by XR, while the surface-parallel structure was studied by GID and Bragg rod (BR) measurements [33,34]. The details of the measurements, analysis, and results are discussed in Sec. III.

C. Surface-tension measurements

The ST measurements were carried out using a two-stage, temperature-controlled sample cell, almost identical to that of the x-ray measurements [13,19]. The Wilhelmy plate method [35] was employed, using an electronic balance and a plate made of filter paper to enhance wetting by the alkane sample. Several of the measurements were repeated using plates made of tantalum foil. The results obtained were in all cases identical with those obtained with the paper plates, within the experimental uncertainties. Cooling below ambient was done using a temperature-stabilized water circulator. The samples were kept at $>10\,°C$ above the melting temperature for ~ 1 h prior to a measurement run, and multiple cooling scans were carried out at each concentration ϕ. As C_{12} is slightly hygroscopic, the ST apparatus was kept inside an enclosure flooded with dry nitrogen throughout the measurements. For comparison, several ST scans were also done with the apparatus open to air. The differences were found to be smaller than the error bars of the measurements.

To avoid contamination, the paper plate was changed for different concentrations, and also for different samples of the same concentration. This introduced a small uncertainty in the measured ST values due to the unavoidable variations in cutting the paper to size. The first few scans measured for a fresh sample showed a monotonic change with time, possibly because of imperfect wetting of the paper plate, and/or incomplete settling of the mixed sample. Saturation of this ''drift'' and complete reproducibility were achieved only after several scans. The results discussed below were derived in all cases from the later scans which were reproducible, and showed no variation with time.

The ST was measured in discrete temperature steps, staying at each step for 30s. This yields an effective scan rate of $10^{-3}\,°C/s$. For each temperature step, an average of 20 measurements was taken within a period of 30 s. In addition to the cooling scans, bidirectional cooling-heating scans were also carried out for several samples, taking care to reverse the direction just before bulk freezing is reached, to avoid possible demixing. These scans show the results to be independent of the scanning direction. Also, as found in pure materials, no hyteresis is detected in the surface-freezing temperatures [13].

III. RESULTS AND DISCUSSION

A. Surface-tension measurements

Typical ST scans $\gamma(T)$ for different molar concentrations ϕ are shown in Fig. 1. The most outstanding feature of these curves is the slope change, upon cooling, from a negative to
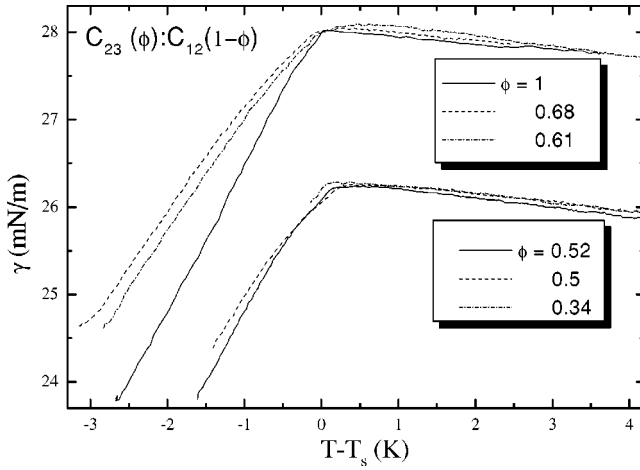
FIG. 1. Surface-tension cooling scans for the C_{23} concentrations listed. The three lowest concentrations are downshifted by 2 mN/m for clarity. Note the sharp break in the curves at T_s, the surface-freezing onset temperature. The curves end at the bulk freezing temperature T_f. The existence range $\Delta T_{SF} = T_s - T_f$ is observed to be roughly constant at 2.5–3 °C for $\phi > 0.6$, and diminishes linearly with decreasing ϕ for $\phi < 0.6$. Since the measurement errors in the absolute surface-tension values are no better than ~ 1 mN/m, all curves were shifted by small amounts to have their surface-tension values at T_s coincide.

a positive value as the surface-frozen layer is formed at $T = T_s$. The surface tension is a direct measure of the surface excess free energy [35]:

$$\gamma(T) = \varepsilon_s - \varepsilon_b - T(S_s - S_b), \qquad (1)$$

where ε_s and ε_b are the energies and S_s and S_b, the entropies per unit area of the surface and the bulk, respectively. The temperature derivative of surface tension yields informa-

tion on the surface excess entropy $d\gamma/dT = -(S_s - S_b)$, which is a direct measure of the ordering of the molecules on the surface. For ordinary liquid surfaces, the molecules on the surfaces are less constrained than those in the bulk and thus $S_s > S_b$, yielding $d\gamma/dT < 0$. Indeed, a negative temperature slope has been observed for $\gamma(T)$ of all simple liquid surfaces. Upon surface freezing, however, S_s of the (solid) surface becomes smaller than S_b of the (liquid) bulk, and the slope changes sign: $d\gamma/dT > 0$. The temperature range of existence of the surface-frozen layer, $\Delta T_{SF} = T_s - T_f$, is terminated at the bulk freezing temperature T_f. As can be observed in Fig. 1, ΔT_{SF} is constant at ~ 3 °C for dilutions $\phi > 0.6$. At lower concentrations, $\phi < 0.6$, a fast reduction in ΔT_{SF} with ϕ is observed, until ΔT_{SF}, and the SF effect vanish for $\phi < 0.34$. The abrupt slope change in $\gamma(T)$ at T_s for $\phi > 0.6$ suggests that the freezing of the surface monolayer is a first-order transition. No significant hysteresis or any near-transition effects were observed for $\phi > 0.6$. These properties are the same as those of pure alkanes [13]. Upon a careful examination of the figure, at smaller concentrations ($0.4 \leq \phi \leq 0.6$) a region of a lower slope can be observed just below T_s for ~ 1 °C. This region is well defined in the first ST scans for a given sample. In later scans it tends to shrink, while the larger-slope, lower-T region expands. Thus, after several scans, the different slope region below T_s can hardly be distinguished. Since no evidence for a different structure was found in these two regions in the x-ray measurements (see below), and the first few scans vary considerably as discussed above, in the following we consider only the single-slope picture, which emerges in the later scans of every series of ST measurements on a given sample. The transition temperatures and entropy changes derived from the measured $\gamma(T)$ curves are summarized in Table I.

Figure 2 shows the surface and bulk phase diagram, i.e., the T_s and T_f values obtained from the ST measurements,

TABLE I. Experimental results obtained in the surface-tension measurements for the different $C_{23}:C_{12}$ alkane mixtures. ϕ is the bulk mole fraction of C_{23}, and T_s and T_f are the surface and bulk freezing temperatures, respectively. ΔS is the entropy change upon surface freezing, as obtained from the slopes of the surface tension vs temperature curve above and below T_s. Surface freezing vanishes at $\phi = 0.34$.

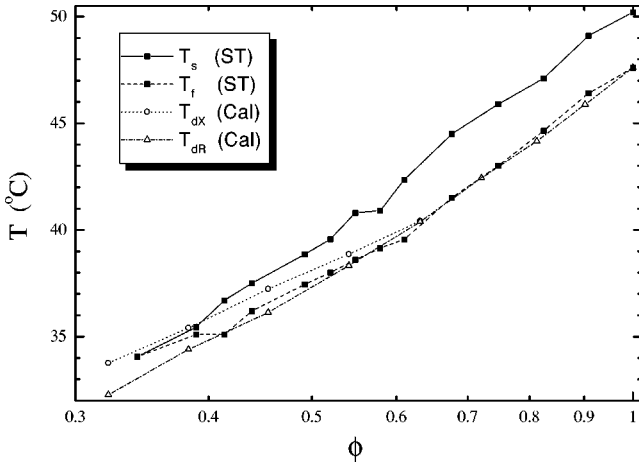| ϕ Mole fraction	T_f (°C)	T_s (°C)	ΔS [mJ/(m^2 K)]
1.0	47.6	50.2	1.73
0.91	46.4	49.1	1.65
0.82	44.7	47.1	1.59
0.75	43.0	45.9	1.45
0.68	41.5	44.5	1.26
0.61	39.6	42.4	1.36
0.58	39.2	40.9	1.7
0.55	38.6	40.8	1.5
0.52	38.0	39.6	1.69
0.49	37.5	38.9	1.48
0.44	36.2	37.5	1.15
0.41	35.1	36.7	1.53
0.39	35.1	35.5	0.5
0.34	34.1		

FIG. 2. The (temperature, concentration) phase diagram of the $C_{23}:C_{12}$ mixtures. T_s and T_f are those obtained from the present ST measurements. T_{dR} and T_{dX} are the dissolution temperatures of the rotator and the crystalline bulk solids, measured using adiabatic calorimetry (Cal) by Sirota [31]. The surface frozen phase vanishes at $\phi = 0.34$. The lines are guides to the eye.

superimposed on the bulk freezing (T_{dR}) and melting (T_{dX}) temperatures measured by adiabatic calorimetry (denoted "cal" in the figure) by one of us (E.B.S.) [31]. T_{dX} and T_{dR} were shown to correspond to the equilibrium crystal-liquid, and rotator-liquid dissolution temperatures, respectively. Indeed, Fig. 2 shows that our measured T_f follow T_{dR}, within the experimental scatter, down to $\phi \approx 0.42$, but increases above T_{dR} at the lowest concentrations. Heterogeneous nucleation by the very existence of a Wilhelmi plate may be responsible for this higher-T nucleation of the bulk, as compared to the adibatic calorimetry results. The lower temperatures and the higher bulk undercoolings ($\delta T = T_{dX} - T_{dR}$) may render the low-$\phi$ range more sensitive to heterogeneous nucleation by this effect. The identical results obtained for paper and tantalum plates, as discussed above, indicate that the filter paper is neither a more nor a less efficient nucleator than the metal. Another possible cause for the reduced supercooling observed at low ϕ in our measurements with respect to those of Sirota [31] could be small temperature gradients inside the cell. While those gradients are small enough to be totally insignificant in determining the temperature, they may enforce positional fluctuations of the particles in the cell, enhancing nucleation in the metastable temperature region. In the absence of those gradients and nucleation sites, ΔT_{SF} should remain nearly constant down to a much lower ϕ, since the T_s curve is nearly parallel to the T_{dR} curve, which is the lower limit of the region of supercooling.

The entropy change upon surface ordering ΔS, is obtained from the measured $\gamma(T)$ curve as

$$\Delta S = (d\gamma/dT)|_{T < T_s} - (d\gamma/dT)|_{T > T_s}. \qquad (2)$$

As Fig. 3(a) shows, ΔS is practically independent of ϕ down to $\phi = 0.4$, within the measurement uncertainty. The smaller ΔS at the lowest concentration, $\phi = 0.39$, is, most probably, due to an incomplete covering of the surface by the ordered
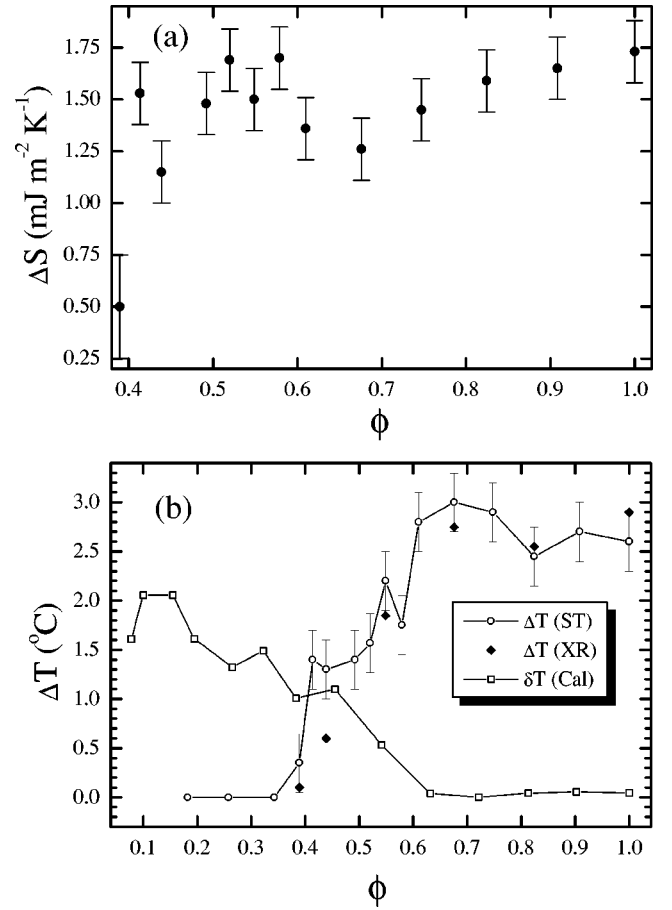

FIG. 3. (a) The entropy change ΔS, upon surface freezing as derived from the slope difference in the surface-tension curves (Fig. 1). ΔS is constant over the full range measured, indicating the surface layer to be a pure C_{23} monolayer. (b) The temperature existence range $\Delta T_{SF} = T_s - T_f$, of the surface-frozen layer as derived from ST measurements and x-ray T scans. The temperature range of undercooling, δT, obtained from adiabatic calorimetry (Cal) by Sirota [31] is also shown. Note that both ΔT_{SF} and δT show a break at $\phi \approx 0.6$, the bulk crossover point from liquid-to-rotator to liquid-to-crystal transitions.

phase. The effect is, however, small and may take the form of an increased disorder at grain boundaries, larger defect concentration within the crystalline structure of the monolayer, etc. The absence of significant changes in ΔS strongly supports the lack of structural phase transitions in the surface-frozen layer with ϕ.

Perhaps the most outstanding feature of the ST and x-ray measurements is shown in Fig. 3(b). ΔT_{SF}, as derived from both the ST and the x-ray measurements, is found to be constant for $\phi > 0.6$, but decreases roughly linearly with ϕ for $\phi < 0.6$. As shown in the figure, the break in $\Delta T_{SF}(\phi)$ occurs at $\phi \approx 0.6$, exactly where the bulk undercooling δT starts rising from zero (also roughly linearly). This threshold in the behavior is clearly related to the triple point, which exists in the phase diagram in Fig. 2 at $\phi \approx 0.6$. At this point a crossover occurs from an equilibrium rotator-liquid melting line (at T_{dR}, for $\phi > 0.6$) to a crystal-liquid melting line (at T_{dX}, for $\phi < 0.6$), as shown in Fig. 2, and on an enlarged scale in Fig. 4.
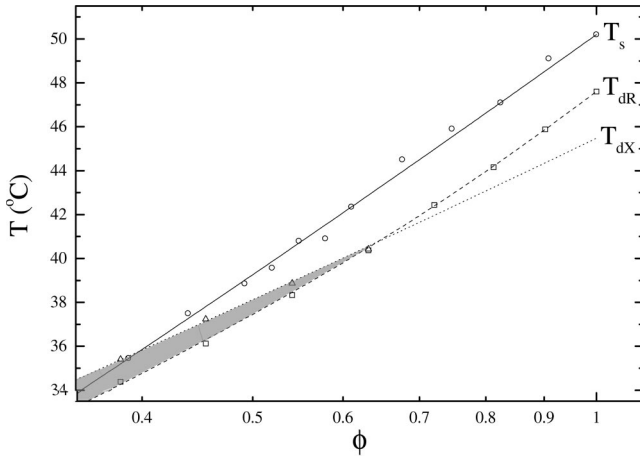
FIG. 4. An enlarged part of the phase diagram in Fig. 2. Note the crossover in the bulk from a crystal-to-liquid dissolution (at T_{dX}) to a rotator-to-liquid dissolution (at T_{dR}) at $\phi = 0.6$. The shading shows the resultant bulk undercooling region. The linear shape of T_s and the upward curving of T_{dR} are clearly observed. This upcurving eventually leads to a pre-emption of the surface freezing by bulk freezing, as discussed in the text. The lines are theoretical fits, based on the theory of ideal solutions. For details see the text.

To account for the ϕ dependence of T_s, and, in particular, clarify its relation to the phase diagram of the bulk, we invoke the general thermodynamics of binary mixtures [36,37], using the properties of the pure components. A similar approach was used previously [31], and shown to account well for the ϕ dependence of the bulk T_{dR} and T_{dX}.

In the liquid phase, the free energy F^l for a mixture of N moles of C_{23} molecules and M moles of C_{12} molecules can be written as [37–39]

$$F^l = N f^l_{23} + M f^l_{12} + k_B T [N \ln(\phi^s) + M \ln(1-\phi^s)]. \quad (3)$$

Here $f^l_i = \varepsilon_i - T S_i$, where $i = 23$ or 12 is the free energy of a C_{23} or C_{12} molecule in a melt of the pure material, S_i is its entropy, and ε_i is its internal energy. The logarithmic terms account for the entropy of mixing. $\phi^s = N/(N+M)$ is the mole fraction of C_{23} in C_{12} at the surface. As discussed below, the surface fraction ϕ^s is, in general, not equal to the bulk fraction ϕ. Rather it is determined by the Gibbs adsorption rule, based on the surface energies of the pure materials. We note that the use of the mole fraction for ϕ here is consistent with common practice in solution theory, and the previous study of the bulk properties of C_{23}:C_{12} alkane mixtures [31]. In an earlier study [15], the Flory mean-field approach, which uses the mass fraction for ϕ (in the liquid phase only) was found to yield a better description for several different long-chain alkane mixtures than the current use of mole fraction for ϕ. However, for the mixtures discussed here, no improvement results from such a definition of ϕ in the fits described below. Thus, here we prefer to use the more common practice of using mole fraction for ϕ. It should also be noted that the mean-fieldlike interchange energy term [37,40] was neglected in Eq. (3) for simplicity, consistently with previous studies [15,31] of long-chain alkane mixtures, where the deviation from nonideality was shown to be negligible in

the liquid phase. Not surprisingly, assuming a nonzero interchange energy (in the mean-field approximation) does not improve the results discussed below.

In the solid phase, the repulsion between C_{23} and C_{12} is known [15] to exceed the phase-separation limit due to the large-chain length mismatch. Since no freezing of C_{12} occurs in our temperature range ($T > 30\,°\text{C}$) [1], and the two compounds do not co-crystallize, the (phase-separated) solid phase consists of pure solid C_{23} alkane [31]. The free energy of such a solid is, of course,

$$F^s = N f^s_{23}. \quad (4)$$

Equating the chemical potential of C_{23} in the two phases $\partial F^l / \partial N = \partial F^s / \partial N$ yields the coexistence temperature on the surface

$$T_s = T^{23}_s + k_B T^{23}_s \ln \phi^s / (\Delta S_{23} - k_B \ln \phi^s), \quad (5)$$

where T^{23}_s and ΔS_{23} are the surface-freezing temperature and entropy change upon surface freezing in the pure C_{23} melt [13]. Equation (5) is independent of the solvent properties. Note also that T_s in Eq. (5) is not strictly linear in $\ln(\phi)$. However, since $\Delta S_{23} \gg k_B \ln \phi^s$, the deviation of T_s from linearity is, in practice, rather small, as can be observed in Fig. 4.

Next, we have to relate the liquid concentration at the surface ϕ^s, to the experimental control parameter—the liquid concentration in the bulk ϕ. Invoking the equality of the chemical potentials of the surface and the bulk while both are liquids yields

$$\phi^s = \phi \Gamma_t / (1 - \phi + \phi \Gamma_t), \quad (6)$$

where

$$\Gamma_t = \exp[(\gamma_{12} A_{12} - \gamma_{23} A_{23})/k_B T] \quad (7)$$

and $\gamma_i = 23$ or 12 are the surface tensions of the pure materials at a given temperature T. A_i with $i = 23$ or 12 denotes the area per molecule in the liquid surface phase of the two pure materials. Equation (6) is the simplest form of the well-known Gibbs adsorption rule [37,38].

Calculations using Eqs. (6) and (7) require an estimate of the effective molecular areas A_{12} and A_{23} of the two constituents in the liquid surface phase. In bulk melts and solutions, it is known that the conformations are given by the rotational isomeric state model unperturbed by neighboring molecules [41,42]. The molecules have *trans-gauche* disorder without significant all-*trans* sequences. For molecules of the chain-lengths used here, this state does not correspond to a random coiled ball conformation, but rather to structures that are kinked, but, nevertheless, highly anisotropic. Thus, the molecules in the liquid have an average extension of approximately 80% of the fully extended length, which corresponds to an average area molecule only 20% higher than the approximately 20 Å^2 characteristic of the ordered phases. In the bulk liquid, there is no long-range order of the orientation of the anisotropic molecule's long axis. There is only short-range packing giving a broad peak at $q = 1.35$ Å^{-1} corre-

sponding to an area of approximately 25 Å^2 per chain for the local packing of chain segments. Nonlinear optics studies [43] show, that even in the liquid surface phase, the surface molecules have finite orientation of their conformation normal to the surface. This may be due to a slight preference for CH_3 groups at the surface [1,24]. Furthermore, a broad GID peak is observed at $q_{||} \approx 1.35$ Å^{-1} at the surface in the liquid surface phase [16]. The above suggests that the effective area molecule at the surface in the liquid phase is 20–25 Å^2, but not a much larger value corresponding, e.g., to the projection of a lying down molecule. This value is further supported by an intercomparison of the measured bulk and surface entropy changes upon freezing (see the Appendix). Thus the molecular area at the surface is similar in both the surface-frozen and liquid surface phases, and roughly independent of the chain length.

Assuming, then, $A_{12} = A_{23} = 20$ Å^2, Eq. (7) depends only on the surface-tension difference $\gamma_{12} - \gamma_{23}$. Neglecting the weak temperature dependence of γ in the liquid phase and using published values [14] for the pure alkanes at 30 °C ($\gamma_{23} = 29.11$ mJ/m^2 and $\gamma_{12} = 24.75$ mJ/m^2) we obtain $\Gamma_t = \exp[-8.72 \times 10^{-22} / k_B T]$. Using this Γ_t in Eqs. (5) and (6), they can be fitted to the measured $T_s(\phi)$ values, varying only ΔS_{23}. The fit result is shown in Fig. 4 in a solid line, along with the fits of corresponding expressions, derived by Sirota [31], for the measured bulk dissolution temperatures T_{dX} and T_{dR}. The shaded region indicates the region where the bulk can be undercooled, bracketed by the T_{dX} and T_{dR} lines. The rather good fit to the measured $T_s(\phi)$ yields $\Delta S_{23} \approx 190$ J/(mole K) or ~ 1.55 mJ/(m^2 K). Although this deviates by approximately 15% from the previous ST-measured [13] 1.32 mJ/(m^2 K), the agreement is still good considering the uncertainties in the determination of the liquid-phase molecular area and the approximations made in the calculations. The present value also agrees well with those in Fig. 3(a) and Table I. While a more sophisticated theory would perhaps yield a better agreement, the discussion above clearly shows that a simple model, based on the theory of ideal solutions, can account reasonably well for the measurements of both the bulk and the surface, based on the same set of reasonable parameter values. An even simpler model would also fit our data reasonably; neglecting the Gibbs adsorption rule (i.e., setting $\phi^s = \phi$) a good fit is obtained with ~ 160 J/mole or ~ 1.3 mJ/(m^2 K), which coincides with the previously measured ST value [13]. More complicated models, based, e.g., on the Flory mean-field approach [15], where $\phi^s = Nn/(Nn + Mm)$, with $n = 23$ and $m = 12$, give similar quality results. We note that if the Flory mean-field approach, which employs the mass fraction, is chosen, the Gibbs rule in Eq. (7) should be rewritten, as shown elsewhere [13,44], yielding a considerably more complicated expression.

Figure 4 demonstrates the reason for the nearly linear decrease observed in Fig. 3(b) in the existence range of the surface-frozen layer ΔT_{SF}. The fact that our surface-freezing curve, $T_s(\phi)$, and Sirota's liquid-rotator transition line $T_{dR}(\phi)$, are almost parallel for $0.6 < \phi < 1$, is a strong indication that both bulk and surface have the same structure, i.e., that the surface-frozen layer is a R_{II} rotator. The x-ray

measurements discussed below indeed confirm this conclusion, not only for $0.6 < \phi < 1$, but down to the lowest concentration showing surface freezing, $\phi \approx 0.34$. However, one distinction exists between the bulk and surface rotators. The surface rotator is a R_{II} phase at all temperatures (and concentrations) studied here, which yields a linear dependence of T_s on $\ln(\phi)$ [31]. By contrast, the bulk R_{II} phase converts to an R_I and then to an R_V upon cooling [7]. As shown by Sirota [31] this leads to a change to lower slopes in the $T_{dR}(\phi)$ curve with decreasing ϕ (and hence also T). A quadratic expression in $\ln(\phi)$ was found to describe the measured $T_{dR}(\phi)$ well. Figure 4 clearly shows the curved $T_{dR}(\phi)$, and the linear $T_s(\phi)$. Since the bulk freezing temperature is essentially identical with T_{dR}, $\Delta T_{SF} = T_s - T_f$ should follow the difference $T_s - T_{dR}$. Because of the upward curving of T_{dR} and the linearity of T_s, the gap between the two lines should decrease, and eventually vanish as they intersect, as indeed is observed. The deviation of T_{dR} from linearity close to $\phi = 1$ is small, so that ΔT_{SF} appears constant within the scatter of the measured points. As ϕ, and thus T, decrease, the upcurving of T_{dR} becomes large and ΔT_{SF} starts decreasing. The intersection, and hence the vanishing of ΔT_{SF}, is expected to occur around $\phi \approx 0.2$. However, the heterogeneous nucleation effects discussed above cause a higher-ϕ vanishing point at $\phi \approx 0.34$.

B. X-ray reflectivity

The surface-normal structure was explored by XR measurements. Figure 5(a) shows the Fresnel (R_F)-normalized XR curve $R(q_z)/R_F(q_z)$ for pure C_{23} and a $\phi = 0.55$ mixture (triangles). Here $q_z = (4\pi/\lambda) \sin \alpha$, where α is the incidence angle relative to the surface and λ is the wavelength of the x rays. The pure C_{23} XR curve is shown at two different temperatures: one above (squares) and one below (circles) the surface-freezing temperature T_s. At the higher temperature, $R(q_z)/R_F(q_z)$ decreases monotonically with q_z, as is typical for a liquid surface [33]. It is well described by $R(q_z)/R_F(q_z) = \exp(-q_z^2 \sigma^2)$, as can be observed from the fitted line. This exponentially decreasing q_z dependence arises from the Gaussian-distributed interfacial roughness σ [33,34,45]. This roughness is mainly due to thermally excited capillary waves [46–48]. Below T_s, modulations suddenly appear in the reflectivity curve, indicating the appearance of a surface layer of a density different from that of the liquid bulk. The modulations are caused by interference between rays reflected from the lower and upper interfaces of the surface-frozen layer. Their period is indicative of the layer's thickness. Fixing q_z at a value corresponding to one of the modulation peaks, one can scan the temperature to study the appearance of the layer. These so-called T scans are shown in Fig. 5(c) for several ϕ values. The surface-freezing onset upon cooling is characterized by a sharp increase in reflectivity, indicating a first-order phase transition. The intensity changes in the reflectivity from the surface-frozen layer at each dilution are insignificant, indicating that no changes occur in the layer structure and surface coverage over the 2–3 °C range of existence of the SF effect.
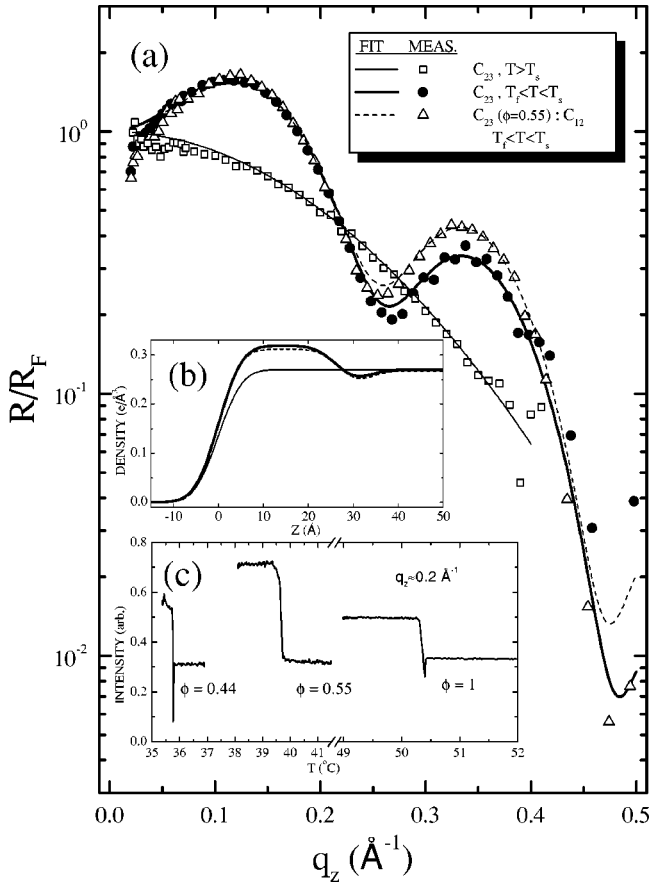
FIG. 5. (a) The Fresnel (R_F)-normalized x-ray reflectivity curves for the samples and phases indicated. Note the difference between the monotonic shape obtained for the liquid surface above T_s and the modulated curves obtained in the surface-frozen phase below T_s. (b) The electron density profiles derived from the fits to the x-ray reflectivities shown by the corresponding lines in (a). The higher-density surface-frozen layer is clearly observed. (c) T scans (reflectivity curves measured at a fixed q_z vs temperature) reveal the onset of surface freezing as an abrupt change in the reflectivity. The magnitude of the change depends on the surface roughness, the q_z value chosen, the temperature, etc.

The XR data were fitted using a layered interface model consisting of a slab of higher electron density, representing the ordered $(CH_2)_{n-2}$ chains, followed by a lower-density depletion zone at the layer-liquid interface, corresponding to the less dense CH_3 groups. This is the same model that was successfully used previously to model the surface-frozen layer of pure alkanes [13,16] and alkane mixtures [15,44]. The bulk electron density at each ϕ was fixed at the value calculated by linear interpolation between the values of pure C_{23} (0.27 e/Å^3) and the pure C_{12} (0.261 e/Å^3) [1]. A single effective roughness (σ) common to all interfaces of a given sample, but varying with ϕ, is assumed. The $(CH_2)_{n-2}$ layer thickness $D(\phi)$, its electron density $\rho(\phi)$, and roughness $\sigma(\phi)$, were allowed to vary in the fit. To minimize the number of fitting parameters, the electron density $\delta\rho$, and the thickness δd, of the CH_3 depletion layer at the liquid-monolayer interface were fixed at the values obtained for pure alkanes [13], $\delta\rho \approx 0.15$ e/Å^3, $\delta d \approx 2.3$ Å. Good fits
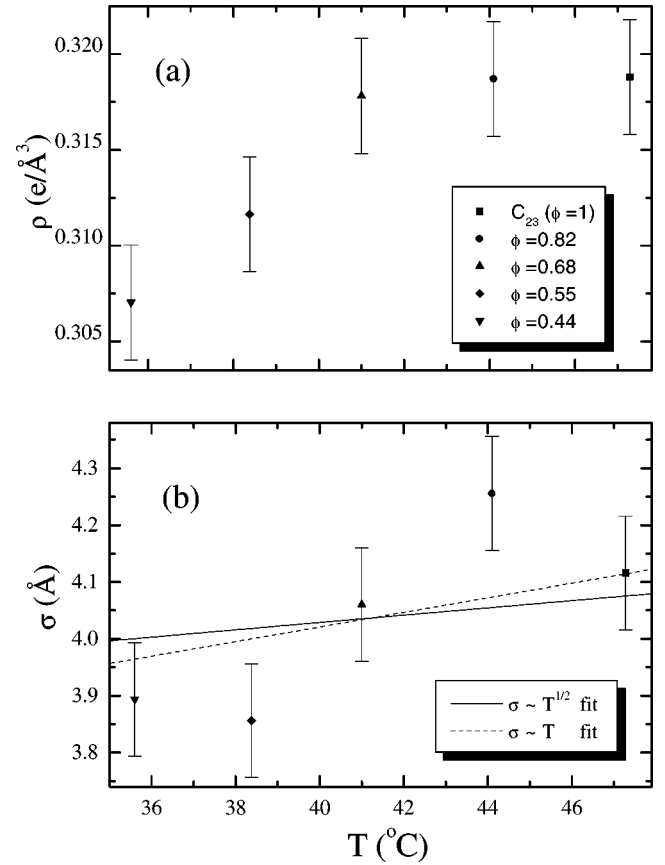
FIG. 6. (a) Densities $\rho(\phi)$ and (b) surface roughness values $\sigma(\phi)$ derived from the fits similar to those shown in Fig. 5(a). Note the slight decrease in the apparent ρ with decreasing ϕ, probably due to incomplete coverage of the surface by the monolayer. The increase in σ with ϕ, in (b) is due to the corresponding increase in the temperature, and the associated capillary-wave roughness. The lines are fits to standard capillary-wave theory (dashed line) and the entropic theory of surface freezing of Tkachenko and Rabin [21,20] (solid line). The later provides a marginally better fit than the former.

were achieved, as shown by the lines in Fig. 5(a). The corresponding density profiles are shown in Fig. 5(b). The monotonic decrease of a typical liquid is observed for C_{23} above T_s. The existence of a surface-frozen layer below T_s for the pure C_{23} and the mixture are shown as well.

Figure 6 summarizes the values obtained from the XR fits for all ϕ measured. The density of the $(CH_2)_{n-2}$ slab, $\rho(\phi)$, is shown in Fig. 6(a). For $\phi \geq 0.6$, the density is constant at the value of the pure material. For $\phi < 0.6$, however, the density seems to decrease slightly, reaching a value 4% below that of the pure C_{23} at the lowest ϕ measured. Since the x-ray results, discussed below, do not indicate any structural changes, and as the positive temperature expansion coefficient should have resulted in an *increase* in the density with decreasing T, the decrease observed is most probably due to incomplete coverage of the sample's surface by the surface-frozen monolayer. A similar reduction in ΔS was also found at the lowest ϕ, and attributed to the same effect, as discussed above.

Figure 6(b) shows the behavior of $\sigma(T)$ at different bulk concentrations. The increase observed in σ with ϕ is attributed to the corresponding increase in temperature. The capillary wave theory [46,48] predicts a square-root increase in the roughness with T, while according to the fluctuation-based entropic scenario [20–22] a linear dependence is expected [49]. The lines in Fig. 6(b) show both theoretical predictions. Though the short T range does not allow a clear distinction between linear and square-root T dependencies, a linear T dependence, predicted by the entropic scenario (dashed line) seems to agree marginally better with the data.

The $(CH_2)_{n-2}$ slab thickness, $D(\phi)$ was found to be constant at 28.3 ± 0.8 Å for all ϕ. D's independence of ϕ supports the conclusion that the surface layer indeed consists of pure C_{23}. The value obtained for D yields a layer thickness of $D + \delta d \approx 28.3 + 2.3 = 30.6$ Å. Within the ± 0.8 Å error of D, this agrees very well with the calculated length l of a fully extended C_{23} molecule: $l = 1.27 \times 21 + 2.27 \times 2 \approx 31.2$ Å [1,13,15,19,44].

C. Grazing incidence diffraction

To probe the structure within the surface plane, grazing incidence diffraction measurements were carried out. The in-plane full width at half-maximum resolution of these measurements, $\Delta q_{||} \approx 6 \times 10^{-3}$ Å^{-1}, was achieved by using Soller slits. Several typical GID scans, for different temperatures and concentrations, are shown in Fig. 7(a). For all samples, a single in-plane peak was observed at $q_{||} \approx 1.52$–1.53 Å^{-1}, indicating a hexagonal packing within the surface plane, as found for pure C_n up to $n \approx 30$ [13]. The peak position corresponds to a nearest-neighbor chain separation in the surface plane of $d = 2\pi/[q_{||}\cos(30°)] \approx 4.77$ Å for our case of hexagonal packing. All GID results are listed in Table II. The peak position decreases with temperature, indicating an increase in the lattice spacing. As discussed above, the surface monolayer is pure C_{23}, and the only change that occurs upon increasing the C_{12} concentration is the depression of the freezing temperature. These mixtures offer, therefore, a unique opportunity to follow the lattice expansion over a very wide temperature range, which is not accessible in the pure material. The nearest-neighbor chain separation in the surface plane d for the measured concentrations and temperatures are shown in Fig. 7(b). d varies linearly with temperature and its slope yields a linear expansion coefficient of $(dd/dT)/d = 6.5 \times 10^{-4}$ °C^{-1}. An identical value was measured for the bulk R_{II} rotator phase [1,50], the structure of which is very similar to that of the surface-frozen monolayer. Our recent high-resolution study [51] of the expansion coefficient of the surface-frozen layer in pure C_{20} yields a similar, though somewhat higher, value of $(dd/dT)/d = (9.0 \pm 1.0) \times 10^{-4}$ °C^{-1}. Although the line in Fig. 7(b) provides a good description of the measured values, the data is not reliable enough to rule out small slope changes with concentration. Indeed, the lower concentration data, which could be measured over a broader temperature range, seems to indicate a larger expansion coefficient. Future high-resolution measurements, where the narrow diffraction peaks will allow smaller
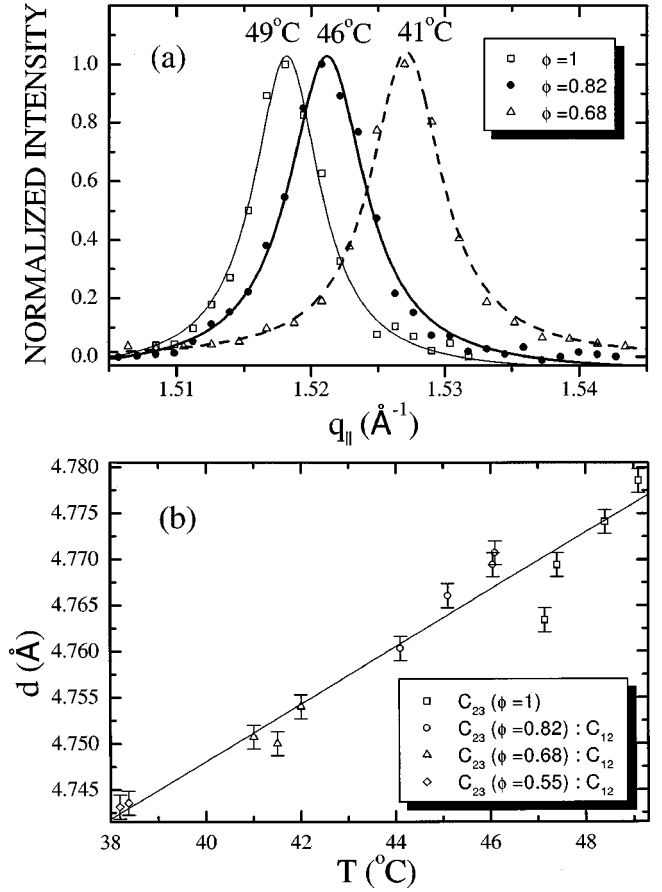

FIG. 7. (a) Measured GID peaks (points) of the surface-frozen monolayer, and Lorentzian fits (lines). The shift in position with temperature is clearly observed. The widths of the peaks yield a coherence length for the in-plane order of at least a few thousand Å. (b) The nearest-neighbor chain separation in the surface plane d, derived from the GID measurements for the various mixtures. The decrease with temperature over an extended range allows fitting by a straight line, the slope of which yields a linear thermal expansion coefficient of $(dd/dT)/d = 6.5 \times 10^{-4}$ °C^{-1}.

peak shifts to be resolved, are required to allow a better determination of possible changes in the expansion coefficient with ϕ.

The area per molecule in the frozen surface layer is obtained from the x-ray measurements as $A_{sx} = 8\pi^2/(\sqrt{3}q_{||}^2)$ which, over our temperature range, varies from 19.5 to 19.8 Å^2. The resultant electron density of the alkyl chain, having 8 electrons per CH_2 group and a projected length of 1.27 Å along the molecular axis, can be estimated directly as $8/(19.75 \times 1.27) = 0.319$ e/Å^3, very close to the densities obtained from the XR fits, shown in Fig. 6(a). Since the reflectivity measurements probe the macroscopic x-ray-illuminated area, averaging over both ordered and (possibly) disordered regions, while the GID probes only the ordered regions, the agreement of the XR and GID derived densities is a strong indication that the surface is completely covered by the ordered monolayer, at least for $\phi > 0.55$, as mentioned above.

The widths of the in-plane GID peaks are shown in Fig. 8. Note that for high T (also high ϕ) the in-plane peaks are

TABLE II. Grazing incidence x-ray diffraction results from measurements on the surface-frozen monolayer for the various C_{23} concentrations (ϕ) and temperatures (T). $q_{||}$ is the peak position of the single GID peak observed, and $d = 4\pi/(\sqrt{3}q_{||})$ is the corresponding in-plane intermolecular distance.

ϕ Mole fraction	T (°C)	$q_{||}$ (Å^{-1})	d (Å)
1.0	49.1	1.518	4.779
	48.4	1.520	4.774
	47.4	1.521	4.769
	47.1	1.523	4.763
0.82	46.1	1.521	4.769
	46.1	1.521	4.771
	45.1	1.522	4.766
	44.1	1.524	4.760
0.68	42.0	1.526	4.754
	41.5	1.527	4.750
	41.0	1.527	4.751
0.55	38.4	1.529	4.744
	38.2	1.530	4.743

resolution limited, indicating that the coherence lengths are at least several thousand Å. The error bar in the individual values is large. However, there appears to be a slight increase in the width at lower temperatures. This is an expected effect since the hexagonal rotator phase consists of local orthorhombic domains with the distortion oriented randomly in all three directions. When the temperature is lowered in the hexagonal phase, the size of the orthorhombic domains grows, causing a packing frustration and a decrease in the degree of positional order in the hexagonal phase. When the transition to the orthorhombic phase occurs, positional order is again restored. This effect was first observed in mixtures of *n* alkanes where the orthorhombic phase was destabilized by decreased interlayer interactions and the hexagonal phase had a wide temperature range [52]. This effect was shown to be
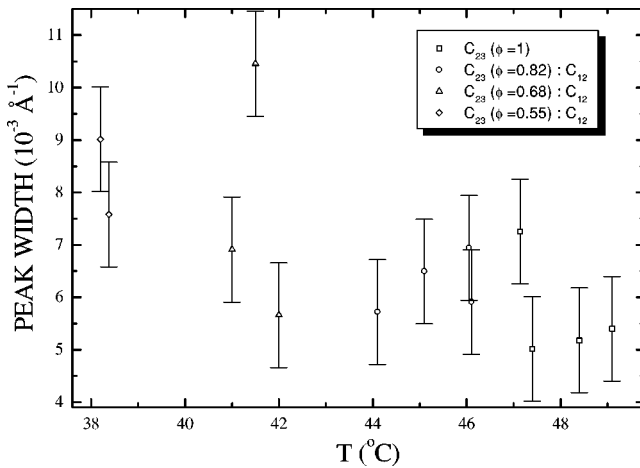

FIG. 8. The widths of the measured grazing-incidence diffraction peaks. Note that while for high temperatures (which correspond to high ϕ) a resolution limited peak is obtained, with a width of 0.006 Å^{-1}, the width seems to increase at lower temperatures. For a discussion see the text.

quite general [8]. Such disorder was also confirmed in the hexagonal phase of Langmuir films [53]. Moreover, this effect is not confined to alkyl-chain molecules, and was also observed recently in the hydrated hexagonal phase of DNA [54]. The precise effect of such disorder will differ depending on whether the phase is three-dimensional (3D) crystalline, 2D crystalline, or hexatic. While in the present case the sharp x-ray diffraction peaks clearly prove the existence of quasi-2D order in the surface-frozen monolayer, our finite resolution does not allow a detailed line shape analysis, which could distinguish the mode by which the correlation function decays with distance.

D. Bragg rod measurements

The intensity distribution along q_z at the in-plane peak position ($q_{||}$), the so called BR's, have been measured with a linear position sensitive detector placed vertically behind the Soller slits. The profile of a typical BR, like that shown in Fig. 9, is determined by the product of the molecular form factor and the structure factor of the hexagonally packed monolayer. The structure factor consists of lines perpendicular to the surface, while the form factor is dependent on the molecular shape. In our case, it is symmetric with respect to the molecular axis. The momentum transfer parallel (normal to) the *molecular axis*, denoted by Q_z ($Q_{||}$), and those parallel (normal to) the *surface normal*, denoted by q_z ($q_{||}$), are related by

$$Q_z = q_z \cos\theta - q_x \sin\theta, \qquad (8)$$

$$Q_{||} = [q_y^2 + (q_z \sin\theta + q_x \cos\theta)^2]^{1/2}, \qquad (9)$$

where θ is the angle of tilt from the surface normal [34,45,46] and q_x (q_y) are perpendicular (parallel) to the diffracted beam's wave vector.
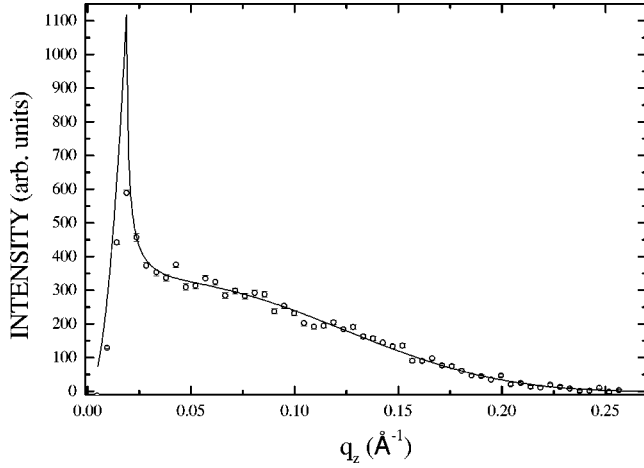
FIG. 9. The Bragg rod measured at the in-plane GID peak position (open circles). A fit (line) to the theoretical expression in the text indicates an extended molecule, with a tilt from the surface normal of no more than 3°.

Multiplying the form factor by the structure factor of a hexagonally packed monolayer of thickness D, the intensity distribution along the BR is given by [45]

$$I(q_z) \propto \left[\left(\frac{\sin(Q_z D/2)}{Q_z D/2} \right)^2 \exp[-(Q_z \sigma_0)^2] \right]$$
$$\times \exp[-(q_z \sigma_z)^2] |T(\alpha)|^2 |T(\beta)|^2. \quad (10)$$

The surface enhancement factors $T(x)$, also known as Vineyard peaks, for the reflection angle $x = \beta$ and the incidence angle $x = \alpha$, are given by

$$|T(x)|^2 = |2 \sin x/(\sin x + \sqrt{\cos^2 \alpha_c - \cos^2 x})|^2, \quad (11)$$

where α_c is the critical angle for total external reflection. When the tilt angle θ is close to zero, our resolution does not allow distinguishing between the surface roughness exponent $q_z \sigma_z$, and the term representing the gradual decrease of the electron density at the molecule's two ends $Q_z \sigma_0$. Thus, the two corresponding terms are lumped into a single term, $\exp[-(q_z \sigma_{eff})^2]$. The fit of Eq. (10) to the measured BR, shown in Fig. 9 as a solid line, yields an effective roughness parameter $\sigma_{eff} \approx 4$ Å, and a layer thickness of $D = 27.8$ Å. Both are very close to, and thus confirm, the values obtained from the XR measurements above. The freely fitted tilt angle is not higher than 3°, with the azimuthal angle of the tilt direction being $\sim 45°$. Because of the very small tilt angle, the value of the tilt direction should not be taken too seriously. This result is also consistent with a nontilted structure.

In conclusion, the x-ray measurements clearly show that the surface-frozen monolayer is an R_{II} rotator for the full range of temperatures explored. By contrast, the bulk rotator phase of C_{23} traverses three different rotator phases, and reaches an orthorhombic crystalline phase, over the same temperature range. The difference in the phase behavior may be due to the interlayer interactions, which are absent in the surface-frozen monolayer, but exists in the case of the bulk crystal. While these interactions are generally considered to be rather weak in rotator phases, they may nevertheless be sufficient to account for the observed difference between the 2D and 3D behavior of C_{23}. This difference merits further attention, and similar studies on other mixtures are indicated.

IV. CONCLUSION

We presented here x-ray and surface-tension studies of surface freezing in C_{23}:C_{12} alkane mixtures. The surface-frozen layer is found to be a pure C_{23} monolayer over the full range of dilutions from $\phi = 1$ (pure C_{23}) to $\phi \approx 0.34$. This corresponds to a ~ 15 °C temperature range. While the bulk crosses over from a liquid-to-rotator transition to a liquid-to-crystal transition at $\phi \approx 0.6$ (at $T = 40.5$ °C), the surface-frozen monolayer preserves its hexagonally packed rotator phase over the whole ϕ range. Its structure is identical with that of a bulk R_{II} rotator phase lamella, and it serves, therefore, as an efficient bulk nucleator from $\phi = 1$ down to $\phi \approx 0.6$, a region where the highest-T equilibrium bulk solid phase is also a rotator phase. The match between the surface and bulk solids eliminates the nucleation barrier, and thus prevents supercooling of the bulk liquid. At $\phi \approx 0.6$, the highest-T solid bulk phase changes from a rotator to an orthorhombic crystal, a structure different from that of the surface-frozen layer. Consequently, the surface-frozen layer no longer promotes bulk nucleation. A nonzero nucleation barrier is established. This, in turn, results in a finite temperature range of supercooling for the bulk, which increases with decreasing ϕ. Consequently, the freezing temperature still follows the extrapolated bulk liquid-to-rotator $T_{dR}(\phi)$ freezing line, as shown by Sirota [31]. A simple model based on ideal solution theory accounts well for the linear dependence of the surface-freezing temperature T_s on $\ln(\phi)$. The vanishing of the surface-freezing effect at low $\phi < 0.3$ results from the pre-emption of surface freezing by bulk freezing, arising from the intersection of the linear $T_s[\ln(\phi)]$ with the quadratic $T_{dR}(\phi)$ of the bulk. The x-ray measurements provide a detailed description of the surface-frozen monolayer and its variation with temperature. In particular, the extended temperature range studied allows an accurate determination of the thermal coefficient of expansion of the surface-frozen layer, which is found to be in reasonable agreement with that of the bulk R_{II} phase. Further measurements on similar mixtures with different chain-length combinations may reveal new surface phases and shed further light on the interplay between the surface and bulk phase behavior and on the details of the solid nucleation in the bulk from solutions and melts.

APPENDIX: COMPARING BULK AND SURFACE ENTROPY CHANGES

Denote by $\widetilde{S}_{ij}$ and A_{ij} the entropy and area *per molecule* at the surface ($i=s$) or in the bulk ($i=b$) in the liquid ($j=l$) or the crystal ($j=x$) phases. The effective entropy change at the surface upon surface freezing *per unit area*, denoted here as ΔG and derived from the measured $\gamma(T)$ curve as the difference in the slopes below and above T_s, is given as

$$\Delta G \equiv (\widetilde{S}_{sl}/A_{sl} - \widetilde{S}_{bl}/A_{bl}) - (\widetilde{S}_{sx}/A_{sx} - \widetilde{S}_{bl}/A_{bl})$$

$$= (\widetilde{S}_{sl}/A_{sl} - \widetilde{S}_{sx}/A_{sx}). \tag{A1}$$

Multiplying now by A_{sx},

$$\Delta G A_{sx} \equiv A_{sx}(\widetilde{S}_{sl}/A_{sx} - \widetilde{S}_{sx}/A_{sx} + \widetilde{S}_{sl}/A_{sl} - \widetilde{S}_{sl}/A_{sx})$$

$$= \widetilde{S}_{sl} - \widetilde{S}_{sx} + \widetilde{S}_{sl}[(A_{sx} - A_{sl})/A_{sl}]$$

$$= \Delta \widetilde{S}_s + \widetilde{S}_{sl}[(A_{sx} - A_{sl})/A_{sl}]. \tag{A2}$$

The bulk entropy change upon freezing of C_{23} was measured by calorimetry to be 164 J/(mole K) [1,55–57], which is $\sim 20\,k_B$ per molecule. The surface entropy change upon freezing, ΔG, was measured independently in surface-tension measurements [13] to be 1.32 mJ/(m^2 K), which is $\sim 1\,k_B$ Å^{-2}. The x-ray measurements above yield $A_{sx} \approx 20$ Å^2. Thus, $\Delta G A_{sx} \approx 20\,k_B$, which is equal to $\Delta \widetilde{S}_b$. This implies

$$\Delta \widetilde{S}_b \approx \Delta \widetilde{S}_s + \widetilde{S}_{sl}[(A_{sx} - A_{sl})/A_{sl}], \tag{A3}$$

where $\Delta \widetilde{S}_b$ and $\Delta \widetilde{S}_s$ are the entropy changes per molecule at the bulk and at the surface. Making now the reasonable assumption that the entropy change upon freezing *per molecule* at the surface and in the bulk are roughly the same [13], requires the second term in Eq. (A3) to vanish and thus leads to the conclusion that $A_{sl} \approx A_{sx} \approx 20$ Å^2.

---

[1] D.M. Small, *The Physical Chemistry of Lipids* (Plenum, New York, 1986).

[2] E.B. Sirota and D.M. Singer, J. Chem. Phys. **101**, 10 873 (1994).

[3] E.B. Sirota, Langmuir **14**, 3133 (1998).

[4] J. Doucet, I. Denicolo, and A. Craievich, J. Chem. Phys. **75**, 1523 (1981).

[5] E. Ewen, G.R. Strobl, and D. Richter, Faraday Discuss. Chem. Soc. **69**, 19 (1980).

[6] G. Ungar, J. Phys. Chem. **87**, 689 (1983).

[7] E.B. Sirota *et al.*, J. Chem. Phys. **98**, 5809 (1993).

[8] E.B. Sirota, Langmuir **13**, 3849 (1997).

[9] E.B. Sirota *et al.*, J. Phys. Chem. **99**, 798 (1995).

[10] A.R. Gerson and S.C. Nyburg, Acta Crystallogr., Sect. B: Struct. Crystallogr. Cryst. Chem. **50**, 252 (1994).

[11] D.L. Dorset, Macromolecules **23**, 623 (1990).

[12] M. Dirand, V. Chevallier, E. Provost, *et al.*, Fuel **77**, 1253 (1998).

[13] B.M. Ocko *et al.*, Phys. Rev. E **55**, 3164 (1997).

[14] X.Z. Wu *et al.*, Science **261**, 1018 (1993).

[15] X.Z. Wu *et al.*, Phys. Rev. Lett. **75**, 1332 (1995).

[16] X.Z. Wu *et al.*, Phys. Rev. Lett. **70**, 958 (1993).

[17] J.C. Earnshaw and C.J. Hughes, Phys. Rev. A **46**, R4494 (1992).

[18] C.J. Hughes and J.C. Earnshaw, Phys. Rev. E **47**, 3485 (1993).

[19] O. Gang *et al.*, Phys. Rev. E **58**, 6086 (1998).

[20] A.V. Tkachenko and Y. Rabin, Phys. Rev. E **55**, 778 (1997).

[21] A.V. Tkachenko and Y. Rabin, Phys. Rev. Lett. **76**, 2527 (1996).

[22] A.V. Tkachenko and Y. Rabin, Phys. Rev. Lett. **79**, 532 (1997).

[23] E.B. Sirota *et al.*, Phys. Rev. Lett. **79**, 531 (1997).

[24] F.A.M. Leermakers and M.A. Cohen Stuart, Phys. Rev. Lett. **76**, 82 (1996).

[25] M. Kawamata and T. Yamamoto, J. Phys. Soc. Jpn. **66**, 2350 (1997).

[26] H. Kraack, M. Deutsch, and E.B. Sirota, Macromolecules **33**, 6174 (2000).

[27] H. Kraack, E.B. Sirota, and M. Deutsch, J. Chem. Phys. **112**, 6873 (2000).

[28] H. Kraack, E. B. Sirota, and M. Deutsch, Polymer **42**, 8225 (2001).

[29] R. Bar-Ziv and S.A. Safran, Phys. Rev. E **49**, 4306 (1994).

[30] A. Weinstein and S.A. Safran, Phys. Rev. E **53**, R45 (1996).

[31] E.B. Sirota, J. Chem. Phys. **112**, 492 (2000).

[32] M. Gavish *et al.* Science **250**, 973 (1990).

[33] M. Deutsch and B.M. Ocko, in *Encyclopedia of Applied Physics*, edited by G.L. Trigg (VCH, New York, 1998), Vol. 23, p. 479.

[34] M.L. Schlossman and P.S. Pershan, in *Light Scattering by Liquid Surfaces and Complementary Techniques*, edited by D. Langevin (Dekker, New York, 1990), p. 365.

[35] G.L. Gaines, *Insoluble Monolayers at the Liquid Gas Interface* (Wiley, New York, 1966).

[36] L.E. Reichl, *A Modern Course in Statistical Physics* (University of Texas, Arlington, 1980).

[37] E.A. Guggenheim, *Mixtures* (Oxford University, Oxford, 1952).

[38] R. Defay *et al.*, *Surface Tension and Adsorption* (Wiley, New York, 1966).

[39] P. Flory, *Principles of Polymer Chemistry* (Cornell, Ithaca, 1953).

[40] J.H. Hildebrand and R.L. Scott, *The Solubility of Nonelectrolytes* (Reinhold, New York, 1950).

[41] M. Dettenmaier, J. Chem. Phys. **68**, 2319 (1978).

[42] D.Y. Yoon and P.J. Flory, J. Chem. Phys. **69**, 2536 (1978).

[43] G.A. Sefler *et al.*, Chem. Phys. Lett. **235**, 347 (1995).

[44] O. Gang *et al.*, (unpublished).

[45] J. Als-Nielsen and K. Kjaer, in *Phase Transitions in Soft Condensed Matter*, edited by T. Riste and D. Sherrington (Plenum, New York, 1989).

[46] A. Braslau *et al.*, Phys. Rev. A **38**, 2457 (1988).

[47] B.M. Ocko *et al.*, Phys. Rev. Lett. **72**, 242 (1994).

[48] M.K. Sanyal *et al.*, Phys. Rev. Lett. **66**, 628 (1991).

[49] O. Gang, Ph.D. thesis, Bar-Ilan University, Israel, 1999 (unpublished).

[50] E.B. Sirota, D.M. Singer, and H.E. King, Jr., J. Chem. Phys. **100**, 1542 (1994).

[51] B.M. Ocko *et al.*, Phys. Rev. E **63**, 032602 (2001).

[52] E.B. Sirota *et al.*, Phys. Rev. Lett. **68**, 492 (1992).

[53] V.M. Kaganer *et al.*, Phys. Rev. E **59**, 2141 (1999).

[54] H.H. Strey *et al.*, Phys. Rev. Lett. **84**, 3105 (2000).

[55] P. Barbillon *et al.*, J. Chem. Phys. **88**, 91 (1991).

[56] Y. Jin and B. Wunderlich, J. Phys. Chem. **95**, 9000 (1991).

[57] G.S. Parks *et al.*, J. Am. Chem. Soc. **71**, 3386 (1949).